PERSPECTIVE

Rydberg antiblockade regimes: Dynamics and applications

View the article online for updates and enhancements.

Perspective

Rydberg antiblockade regimes: Dynamics and applications

S.-L. Su[1] , F.-Q. Guo[1], J.-L. Wu[2], Z. Jin[3], X. Q. Shao[4] and S. Zhang[2,5]

[1] *School of Physics, Zhengzhou University - Zhengzhou 450001, China*
[2] *School of Physics, Harbin Institute of Technology - Harbin 150001, China*
[3] *School of Physics, Northeast University - Shenyang 110819, China*
[4] *Center for Quantum Sciences and School of Physics, Northeast Normal University - Changchun 130024, China*
[5] *Department of Physics, Yanbian University - Yanji 133002, China*

Abstract – Rydberg antiblockade (RAB) allows more than one Rydberg atom to be excited in the presence of Rydberg-Rydberg interaction (RRI) and has many potential applications in quantum optics, many-body physics and quantum information. In this paper, we would review the conditions and possible applications of different types of RAB regimes under weak, intermediate and strong RRIs, respectively. Both van der Waals (vdW) and dipole-dipole (DD) interactions are considered for each interaction strength. This work displays the layout of RAB and provides a reference for further study of RAB-regime-based quantum optics and quantum information processing tasks.

Introduction. – Neutral atoms have strong dipole-dipole or van der Waals interactions when they are excited to Rydberg states and close enough [1–4]. These strong interactions would induce the blockade effect during the excitation process [5–7], because the collectively excited Rydberg states would be shifted by some amount of energy induced by the Rydberg-Rydberg interaction (RRI). Since the RRI depends on the inner states of neutral atoms, the conditional dynamics can be easily constructed directly in the Rydberg atom system [4,8]. Experimentally, the Rydberg blockade has been observed [9,10]. Along with the recent experimental progresses in quantum computation [11–20], Rydberg atoms become increasingly competitive in constructing quantum computers.

Totally different from the Rydberg blockade regime, the Rydberg antiblockade (RAB), which allows more than one Rydberg atom to be excited, has been studied initially in theory [21] and demonstrated in experiment [22]. Then, ref. [23] showed that the three-atom RAB can be achieved once the dark state containing three excited Rydberg atoms is populated. Also, the two-qubit case where the atoms interact with a zero-area phase-jump pulse was studied [24]. After these seminal works, there has been growing interest recently in RAB based on the concise and accurate RAB dynamics in two- or many-body Rydberg atoms [25,26] via the perturbation theory. This kind of RAB regime has been used to study the motional effects [27], dissipative dynamics-based entangled state production [28–39], periodically driving [40] as well as construction of quantum gates [41–49]. Through Stark-tuned Förster resonance, refs. [50–52] studied another kind of RAB with dipole-dipole (DD) interaction, which is used to construct fast quantum gates. Very recently, RAB was also studied in the strongly interacting Rydberg atom experiment [53], trapped Rydberg ion chain [54], cold atom ensemble [55] and many-body spin-phonon system [56,57].

In this paper, we would review the RAB regimes under strong, intermediate and weak RRI strength cases, respectively. For each case we consider both the vdW-type and DD-type interactions. The condition to realize RAB and the possible applications of RAB are discussed, respectively. This review would be helpful for studying RAB-based quantum optics as well as quantum information processing in theory and experiment.
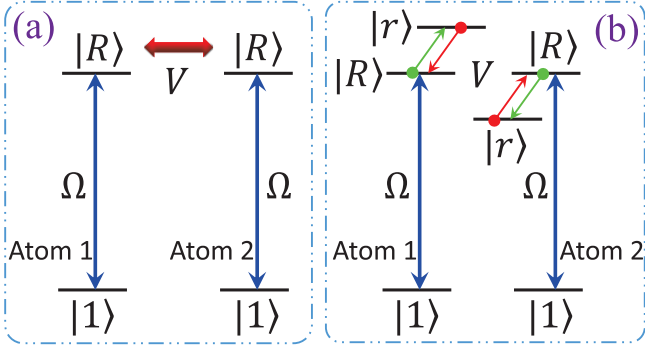
Fig. 1: Energy levels and laser couplings to achieve the RAB with weak RRI strength $V \ll \Omega$. $|1\rangle$ is the ground state. $|R\rangle$ and $|r\rangle$ denote the Rydberg states. V is the RRI strength, Ω is the driving Rabi frequency. Panels (a) and (b) describe the vdW- and dipole-dipole-type RRI, respectively.

RAB with weak RRI strength. –

Dynamics. When the RRI is weak enough, *i.e.*, $V \leq 0.1\Omega$ (here, Ω denotes the Rabi frequency), the RRI almost has no influence on the excitation process, and RAB would appear naturally [3]. We consider two Rydberg atoms interacting with each other through vdW-type RRI (as shown in fig. 1(a)) and DD-type RRI (as shown in fig. 1(b)), respectively. In the interaction picture, the Hamiltonians of these two models can be written as

$$\hat{H}_v = \left(\sum_{j=1}^{2} \Omega/2 |1\rangle_j \langle R| + \text{H.c.} \right) + V|RR\rangle\langle RR|,$$
$$\hat{H}_d = \sum_{j=1}^{2} \Omega/2 |1\rangle_j \langle R| + V|RR\rangle\langle rr| + \text{H.c.}, \tag{1}$$

respectively. Here and throughout this paper, the subscript j denotes the j-th atom, and we take the abbreviation $|mn\rangle$ to denote $|m\rangle_1 \otimes |n\rangle_2$. Through solving the Schrödinger equation $i\dot{\psi} = \hat{H}_{v(d)}\psi$ and using the definition of population $P_{RR} = |\langle\psi|RR\rangle|^2$, we plot $1 - P_{RR}$ in fig. 2 to verify the RAB. The results show that the population of the two-excitation Rydberg state could also be higher than 0.99 with V/Ω equal to 0.1 for both vdW- and DD-type RRIs.

Reference [50] proposed another type of weak-DD-RRI-based RAB via Stark-tuned Förster resonance, and shows how to construct the quantum logic gate based on the proposed regime in ref. [50]. In quick succession, they experimentally demonstrate the resonant RRI [51] and generalize the idea in ref. [50] to a many-body case [52].

Applications. The RAB based on weak vdW-type RRI can be used to construct a quantum gate with three steps [3]. Step i): Exciting two Rydberg atoms from $|11\rangle$ to $|RR\rangle$. Step ii): Turning off the lasers and waiting for a time interval t, and then the phase $\theta = V \times t$ is accumulated on $|RR\rangle$. Step iii): Turning on the lasers again to perform the inverse operation of step i). Through this
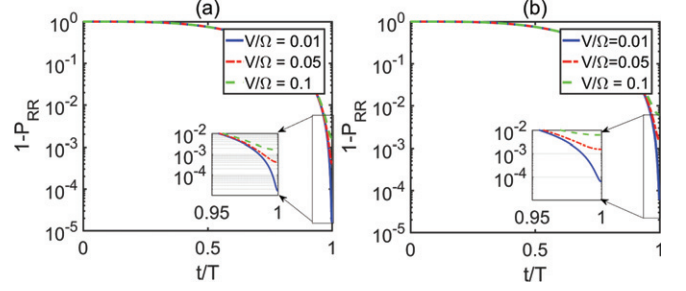

Fig. 2: Population of $|RR\rangle$ with respect to evolution time with vdW-type (panel (a)) and DD-type (panel (b)) RRI, respectively. T is set as π/Ω.

process, $|11\rangle$ gets a phase θ. The weak DD-type RRI-based RAB can also be used to construct a similar gate, but the evolution time in the subspace $\{|RR\rangle, |rr\rangle\}$ should be restricted to make the final state of step ii) be in $|RR\rangle$.

On the other hand, in order to use the RAB regime proposed in refs. [50–52] to construct quantum logic gates, the Rydberg states should be chosen to minimize the RRI initially to avoid the blockade effect. Then the excited Rydberg states are tuned to resonance and the desired phase would be accumulated through this resonant process. Finally the Rydberg states are de-excited to transfer the phase into ground states [50,52].

RAB with intermediate RRI strength. –

Dynamics. Under the parameter range $V \sim \Omega$, the two-excitation Rydberg states cannot be ignored in the process of evolution. On that basis, how to suppress the blockade error is discussed in refs. [58,59] in detail. In this section, we would show the population dynamics based on the intermediate RRI regime via numerically solving the Schrödinger equation. Then we would review the possible applications in quantum logic gates with the rational generalized Rabi cycles [58] or interferentially detuned Rabi cycles [59]. In fig. 3, we plot the population of $|RR\rangle$ *vs.* evolution time. In contrast to the case based on weak RRI, the complete occupation of $|RR\rangle$ cannot be achieved. After investigating this regime more comprehensively, refs. [58,59] proposed how to construct the robust Rydberg quantum logic gates by using the detuned Rabi oscillation.

Applications. Now we briefly introduce the basic thoughts of refs. [58,59] to construct the quantum logic gate with the intermediate RRI. As shown in fig. 4(a), the vdW-type RRI-based scheme requires three steps [58]. Step i): Exciting atom 1 with the Hamiltonian $\hat{H}_1 = \Omega/2 |1\rangle_1 \langle R| + \text{H.c.}$ to achieve the transition $|1\rangle \to |R\rangle$. Step ii): Exciting atom 2 with the Hamiltonian $\hat{H}_2 = \Omega/2 |1\rangle_2 \langle R| + \text{H.c.} + V|R\rangle_1 \langle R| \otimes |R\rangle_2 \langle R|$ to achieve the detuned Rabi cycle $|1\rangle \to |\phi\rangle \to e^{i\theta}|1\rangle$ on atom 2, in which the expressions of $|\phi\rangle$ and the value of θ depend on whether RRI exists or not. Step iii): Performing the inverse operation of Step i). After these three steps, the operations
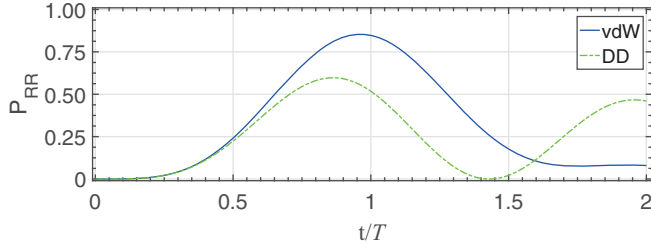
Fig. 3: Population of $|RR\rangle$ with respect to evolution time with vdW- and DD-type RRI, respectively. $T = \pi/\Omega$ and $V = \Omega$ are set.
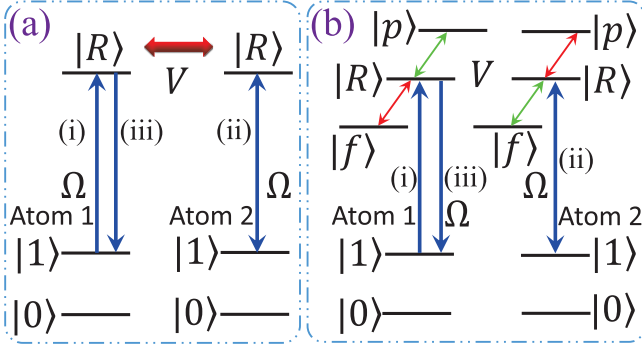

Fig. 4: Energy level and laser driving to construct the quantum logic gate with intermediate RRI strength. $|0\rangle$ and $|1\rangle$ are two ground states. $|R\rangle$, $|p\rangle$ and $|f\rangle$ denote Rydberg states.

$\{|00\rangle \rightarrow |00\rangle, |10\rangle \rightarrow |10\rangle, |01\rangle \rightarrow e^{i\theta_1}|01\rangle, |11\rangle \rightarrow e^{i\theta_2}|11\rangle\}$ are achieved and one can modulate the Ω and evolution time t to get the desired gate. For DD interaction, the schematic diagram is shown in fig. 4(b), and the process is almost the same as that of the vdW interaction. However, since the dynamics of DD-type RRI is more complex than that of vdW-type RRI, the expressions of θ_1 and θ_2 are different from that of the vdW-type RRI-based scheme. And the quantum logic gate can be achieved by modulating the parameters and setting an appropriate evolution time. Then the scheme is generalized to one step case through using the interferentially detuned Rabi cycles to minimize the imperfections of the dephasing error [59].

RAB with strong vdW interaction. – Under strong vdW interaction, *i.e.*, $V \geq 10\Omega$ (Ω denotes the Rabi frequency), the physical diagrams of the Rydberg blockade, RAB with simultaneous and sequential drivings, respectively, are shown in fig. 5. The left rectangle in fig. 5(a) displays the physical diagram of the Rydberg blockade. One can see that the RRI shifts the energy of the two-excitation Rydberg state. Therefore the original frequency mathched pulses cannot excite the two atoms simultaneously. The middle (right) rectangle in fig. 5(a) displays the RAB dynamics with simultaneous (sequential) driving. In the following, we would describe these dynamics in detail.
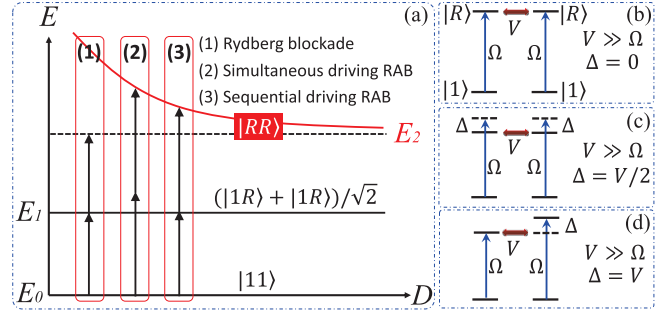

Fig. 5: (a) Illustration of the dynamics of Rydberg blockade (1), RAB with simultaneous driving (2), and RAB with sequential driving (3) under strong vdW-type RRI. D denotes the inter-atomic distance. E denotes the two-atom energy. E_1 (E_2) means the single (two)-excitation state energy. The dashed line denotes the energy of the two-excitation state without considering the RRI. Panels (b), (c) and (d) denote the laser coupling conditions of the Rydberg blockade, RAB with simultaneous driving and sequential driving, respectively.

Simultaneous driving. Before describing the RAB with simultaneous driving, we first show the Rydberg blockade regime induced by RRI. As shown in fig. 5(b), considering two Rydberg atoms driven by classical field resonantly with Rabi frequency Ω. In the interaction picture, the Hamiltonian can be written as (under two-atom basis)

$$\hat{H}_{rb} = \sqrt{2}\Omega/2(|11\rangle\langle T| + |T\rangle\langle RR| + \text{H.c.}) + V|RR\rangle\langle RR|, \tag{2}$$

where $|T\rangle = (|1R\rangle + |R1\rangle)/\sqrt{2}$ denotes the single-excitation state and V denotes the RRI strength. From eq. (2), one can see that the process $|11\rangle \leftrightarrow |T\rangle$ is resonant while $|T\rangle \leftrightarrow |RR\rangle$ is detuned by V. If the condition $V \gg \Omega$ is fulfilled, the two-excitation state $|RR\rangle$ is blocked.

If we replace the resonant interactions by dispersive interactions with detuning Δ, Hamiltonian (2) can be rewritten as

$$\hat{H}_{rab}+ = \frac{\Omega}{\sqrt{2}}[(|11\rangle\langle T|+|T\rangle\langle RR|)e^{i\Delta t}+\text{H.c.}]+V|RR\rangle\langle RR|. \tag{3}$$

Then, if $\Delta = V/2$ is satisfied, the effective Hamiltonian would be

$$\hat{H}_{\text{eff}} = \frac{\Omega^2}{2\Delta}|11\rangle\langle RR| + \text{H.c.} + \hat{S}, \tag{4}$$

where $\hat{S}$ denotes Stark shifts. In fig. 6, we plot the populations of $|RR\rangle$ with full and effective Hamiltonians, respectively. These two curves fit each other very well and both of them approach to unit at the predicted time, which means the RAB can be achieved under strong vdW-type RRI.

This RAB dynamics with strong vdW interaction has been well studied in refs. [25,26] via the second-order perturbation theory and used to study the motional effects [27], dissipation-based quantum state engineering [28–39], periodically driving [40] as well as quantum
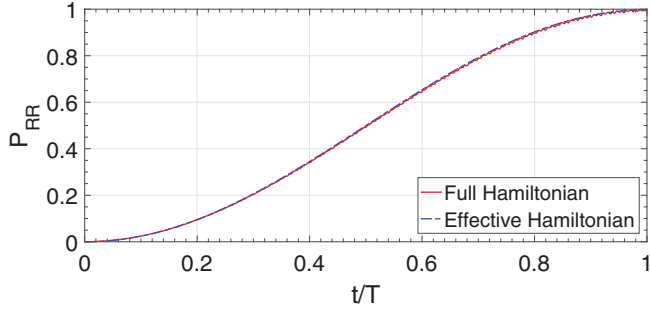
Fig. 6: (a) Numerical plot of the population of $|RR\rangle$ *vs.* evolution time with strong vdW-type RRI. The parameters are set as $\Delta = 10\,\Omega$, $V = 2\Delta - \Omega^2/(2\Delta)$, and $T = \Delta\pi/\Omega^2$.
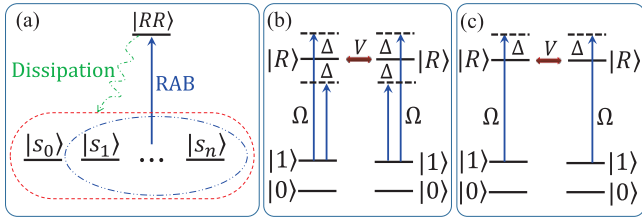

Fig. 7: (a) Illustration of the dynamics of dissipation-based quantum state preparation via RAB. The red dashed, stadium-track-like circle denotes the ground-state subspace $\{|S_0\rangle \cdots |S_n\rangle\}$, in which $|S_0\rangle$ is the target state. The blue dot-dashed ellipse denotes the subspace with inner states coupled by microwave or Raman fields. The states inside the blue dot-dashed ellipse would be excited via RAB, and the two-excitation state would decay to the ground-state subspace via dissipation. Along with the time growth, the population of the desired state increases. (b) The energy level and laser driving to construct the one-step RRI gate via RAB [41] with the antiblockade condition $V = 2\Delta - \Omega^2/(2\Delta)$. (c) The energy level and laser driving to construct the one step RRI gate via the modified RAB condition $V = 2\Delta - \mu\Omega^2/(2\Delta)$, where one can set the values of μ to realize different quantum information processing tasks [42].

computation [41–49]. For the dissipation-based quantum state engineering, ground state $|0\rangle$ should be considered, and the coupling between two ground state should be designed skillfully [28,60,61] to create a unique steady state of the system. The dynamical process for the dissipation-based entangled state preparation with the RAB regime is shown in fig. 7(a). For a quantum logic gate, the other computational basis $|0\rangle$ is also required, and the laser coupling should be designed carefully [41,42], as shown in figs. 7(b) and (c).

In addition, this regime can also be generalized to resonant driving [45,46], and the many-body case [43,62]. Next, this regime is used to construct robust quantum logic gates via holonomic operations [48]. Very recently, the RAB with vdW has also been studied in many-body spin-phonon systems [56,57], open systems [63] as well as in quantum simulators [64]. Especially, in ref. [56], the authors show how to use the spin-phonon interactions and

RAB to generate the tunable many-body interaction. On that basis, the phase diagram in the classical limit was also studied for the isotropic square lattice. In ref. [57], the RAB is employed to facilitate the dynamics and get the desired transitions in the many-body configuration.

Sequential driving. The dynamics of simultaneous driving with strong vdW discussed above is based on two- or higher-order perturbation theory. If we can achieve the RAB with the resonant zero-order interaction, the required time of the excitation process would be reduced and the robustness would be enhanced with the decoherence environment.

The basic dynamical process of sequential-driving-based RAB with vdW-type RRI is discussed in detail in ref. [49], and the dynamical diagram is shown in fig. 8(a). Firstly, driving atom 1 resonantly with Rabi frequency Ω. The interaction Hamiltonian is $\hat{H}_1 = \Omega/2|1\rangle\langle R| + \text{H.c.}$ After a π pulse, the transition $|1\rangle \rightarrow |R\rangle$ is achieved. Secondly, exciting atom 2 with Hamiltonian $\hat{H}_2 = \Omega/2|1\rangle\langle R|e^{i\Delta t} + \text{H.c.}$ and the RAB condition for sequential driving is $\Delta = V \gg \Omega$. If atom 1 is excited, the Hamiltonian with the two-atom basis can be written as $\hat{H} = |R1\rangle\langle RR|e^{i\Delta t} + \text{H.c.} + V|RR\rangle\langle RR|$. Then, after a π pulse, the two-atom excitation state $|RR\rangle$ would be achieved. Otherwise, the state of atom 2 would remain invariant because of the large detuning coupling. This regime was also generalized to the multiple-qubit case [49].

This regime can be used to construct the fast quantum logic gate with three steps, as shown in fig. 8(b). The first step is to resonantly excite $|1\rangle$ to $|R\rangle$ of the control atom via π pulse. The second step is to dispersively apply a 2π pulse on the target atom to couple $|1\rangle$ with $|R\rangle$. The detuning satisfies the RAB condition $\Delta = V$. The last step is the inverse operation of the first step to realize $|R\rangle \rightarrow |1\rangle$ of the control atom. After these three steps, only the state $|11\rangle$ gets a π phase. Besides, the Rydberg excitation superatom to minimize the blockade error can also be achieved [49] based on this sequential driving RAB. The multi-qubit Rydberg numerical results of antiblockade under sequential driving are shown in fig. 9.
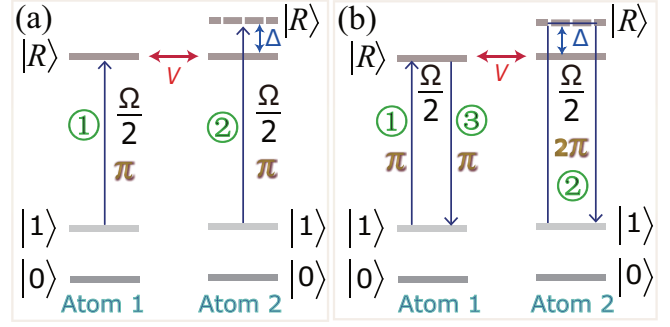

Fig. 8: (a) The energy level and laser driving to achieve RAB with strong vdW-type RRI based on sequential driving. (b) The quantum logic gate via the sequential driving regime. The number in the circle denotes the operation step [49].
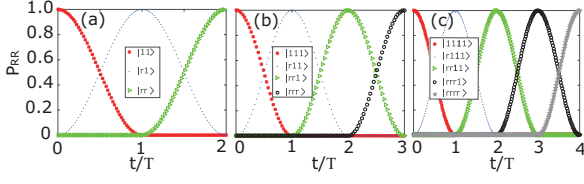
Fig. 9: The numerical results of population *vs.* evolution time with strong vdW-type RRI based on sequential driving. (a) Two-qubit case. (b) Three-qubit case. (c) Four-qubit case. $T = \pi/\Omega$, $V = 10\,\Omega$. The RAB condition is $\Delta_i = (i-1)V$ [49], where i denotes the i-th Rydberg atom.

RAB with strong DD interactions. –

Simultaneous driving. As shown in fig. 10, the resonant DD-type RRI can be roughly divided into two types, one involving three Rydberg states in each atom, as shown in fig. 10(a), while the other containing two Rydberg states, as shown in fig. 10(b). The RAB with these two kinds of RRIs is discussed detailedly in ref. [65]. In the following, we would briefly review these processes.

Reference [65] considers how to achieve the RAB with energy level shown in fig. 10(a). Two lasers are required to illuminate the Rydberg atoms to drive the transition $|1\rangle \leftrightarrow |d\rangle$ with an identical Rabi frequency Ω but opposite detuning Δ. The Hamiltonian in the interaction picture with rotating-wave approximation is $\hat{H} = \hat{H}_\Omega + \hat{H}_V$ [65], in which

$$\hat{H}_\Omega = \frac{\Omega}{2}(e^{i\Delta t} + e^{-i\Delta t})(|1\rangle_1\langle R| + |1\rangle_2\langle R|) + \text{H.c.},$$
$$\hat{H}_V = \sqrt{2}V|RR\rangle\langle r_{pf}| + \text{H.c.}, \qquad (5)$$

where $|r_{pf}\rangle \equiv (|pf\rangle + |fp\rangle)/\sqrt{2}$. In the two-atom basis, the Hamiltonian (5) can be rewritten as

$$\hat{H}_\Omega = \frac{\Omega}{\sqrt{2}}\left(e^{i\Delta t} + e^{-i\Delta t}\right)\left[|11\rangle\langle\Psi| + \frac{1}{\sqrt{2}}|\Psi\rangle(\langle +| + \langle -|)\right]$$
$$+ \frac{\Omega}{2}\left(e^{i\Delta t} + e^{-i\Delta t}\right)(|01\rangle\langle 0R| + |10\rangle\langle R0|) + \text{H.c.}$$
$$\hat{H}_V = \sqrt{2}V(|+\rangle\langle +| - |-\rangle\langle -|), \qquad (6)$$

where $|\Psi\rangle \equiv (|1R\rangle + |R1\rangle)/\sqrt{2}$ and $|\pm\rangle \equiv (|RR\rangle \pm |r_{pf}\rangle)/\sqrt{2}$. From eq. (6), we can understand the Rydberg blockade with DD interaction and can know how to get the RAB condition. When $\Delta = 0$, although $\hat{H}_\Omega$ describes resonant interactions, the total Hamiltonian indicates that the two-excitation Rydberg states would be blocked due to the energy shift induced by RRI when $V \gg \Omega$ is satisfied. To achieve the RAB, we rotate eq. (6) with respect to $\hat{H}_V$. If the conditions $\Delta \gg \Omega$ and $V = \sqrt{2}\Delta - \Omega^2/(3\sqrt{2}\Delta)$ are satisfied, the effective form of eq. (6) in the rotating frame with respect to $e^{-i\hat{H}_V t}$ can be achieved as [65]

$$\hat{H}_e = \frac{\sqrt{2}\Omega^2}{4\Delta}|11\rangle(\langle +| - \langle -|) + \text{H.c.} \qquad (7)$$

From eq. (7), one can see that the state $|11\rangle$ is resonantly coupled to the two-excitation Rydberg state with the effective Rabi frequency $\Omega_{\text{eff}} \equiv \Omega^2/(\sqrt{2}\Delta)$, which indicates that the RAB is achieved.
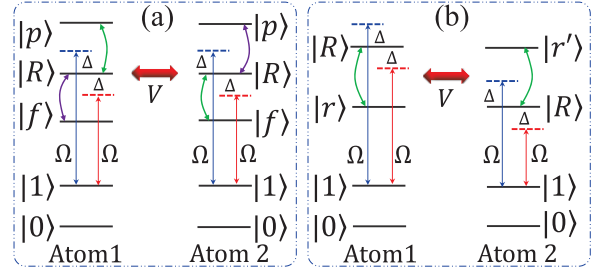

Fig. 10: The diagrammatic sketch of the RAB with resonant dipole-dipole interactions [65]. (a) The laser drivings to achieve the RAB with the resonant DD-type RRI Hamiltonian $\hat{H} = V|RR\rangle(\langle pf| + \langle fp|) + \text{H.c.}$ (b) The laser coupling to achieve the RAB with the resonant DD-type RRI Hamiltonian $\hat{H} = V|RR\rangle\langle rr'| + \text{H.c.}$ V and Ω denote the RRI strength and Rabi frequency, respectively. $|p\rangle, |R\rangle, |f\rangle, |r'\rangle$ denote Rydberg states. $|0\rangle$ and $|1\rangle$ are two ground states.

We now review the basic dynamics of the RAB with energy levels shown in fig. 10(b). Consider the Rydberg atom 1 (2) with two ground states $|0\rangle$ and $|1\rangle$ as well as two Rydberg states $|R\rangle$ and $|r\rangle$ ($|r'\rangle$). Two lasers drive off-resonantly the atoms to achieve $|1\rangle \leftrightarrow |R\rangle$ with an identical Rabi frequency Ω but opposite detuning Δ. After the rotating-wave approximation, the Hamiltonian can be written as [65]

$$\hat{H}_\Omega = \frac{\Omega}{2}\left(e^{i\Delta t} + e^{-i\Delta t}\right)(|1\rangle_1\langle R| + |1\rangle_2\langle R|) + \text{H.c.},$$
$$\hat{H}_V = V|RR\rangle\langle rr'| + \text{H.c.} \qquad (8)$$

Through using the dressed states $|\widetilde{\pm}\rangle \equiv (|RR\rangle \pm |rr'\rangle)/\sqrt{2}$, one can rewrite eq. (8) as

$$\hat{H}_\Omega = \frac{\Omega}{\sqrt{2}}\left(e^{i\Delta t} + e^{-i\Delta t}\right)\left[|11\rangle\langle\Phi| + \frac{1}{\sqrt{2}}|\Phi\rangle(\langle\widetilde{+}| + \langle\widetilde{-}|)\right]$$
$$+ \frac{\Omega}{2}\left(e^{i\Delta t} + e^{-i\Delta t}\right)(|01\rangle\langle 0d| + |10\rangle\langle d0|) + \text{H.c.},$$
$$\hat{H}_V = V(|\widetilde{+}\rangle\langle\widetilde{+}| - |\widetilde{-}\rangle\langle\widetilde{-}|) \qquad (9)$$

with $|\Phi\rangle \equiv (|1R\rangle + |R1\rangle)/\sqrt{2}$. If the relation $\Delta \gg \Omega$ and RAB condition $V_d = 2\Delta - \Omega^2/(3\Delta)$ are satisfied, one can get the effective Hamiltonian as [65]

$$\hat{H}_e = \frac{\Omega^2}{2\Delta}|11\rangle\langle\widetilde{+}| - \langle\widetilde{-}| + \text{H.c.}, \qquad (10)$$

which means the Rabi oscillation between $|11\rangle$ and the two-excitation Rydberg state emerges. If one chooses the evolution time $t = \pi\Delta/\Omega^2$, the RAB would be implemented.

In fig. 11, we plot the populations of $|11\rangle$, $|+\rangle$ and $|-\rangle$ *vs.* time by using the full Hamiltonian without considering the $|0\rangle$ state. One can see that the RAB can be realized at the predicted time. As discussed in ref. [65], this regime can be used to realize geometric quantum computation, dissipative-dynamics-based entanglement preparation, and rough estimation of physical parameters. One can also apply the shortcut-to-adiabaticity
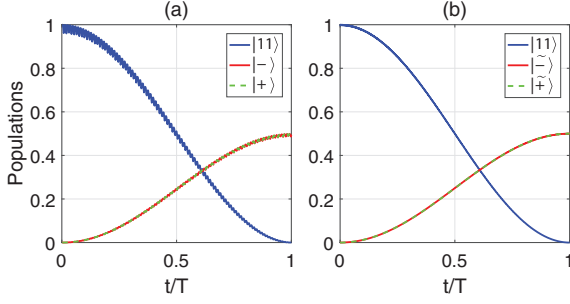
Fig. 11: (a), ((b)) Numerical results of the strong DD-type RRI-based RAB with the energy levels shown in fig. 10(a), ((b)). For panel (a), the parameters are set as $\Delta = 13.3\,\Omega$ and $V = \sqrt{2}\Delta - \Omega^2/(3\sqrt{2}\Delta)$ (RAB condition). For panel (b), the parameters are set as $\Delta = 29.5\,\Omega$ and $V = 2\Delta - \Omega^2/(3\Delta)$ (RAB condition).

technology [66–68] into the RAB to realize more robust quantum information processing tasks [33].

Dark-state-based RAB with DD-type RRI. In ref. [23], the authors considered to break the blockade regime through using the dark state. They consider three identical Rydberg atoms (atom 1, atom 2, atom 3) that interact with each other through DD interactions. Atom 3 is equidistant between atoms 1 and 2 with interaction strengths $V = V_{13} = V_{23}$ and $V' = V_{12}$. By diagonalizing the Rydberg DD interaction Hamiltonian, one can get the dark state as [23]

$$|m_4\rangle = [V'(|dfp\rangle + |dpf\rangle + |fdp\rangle + |pdf\rangle),$$
$$-2V(|fpd\rangle + |pfd\rangle)]/\sqrt{V'^2 + 2V^2}, \quad (11)$$

where $|p\rangle$, $|d\rangle$, and $|f\rangle$ denote three Rydberg states. For weak fields, the triple-excitation probability monotonically decreases with increasing Förster defect and is maximal when the Förster defect is zero, which means that the RAB is achieved [23].

Unconventional Rydberg atom regimes. Differently from all of the above RAB regimes and the conventional Rydberg blockade regime [3,4], refs. [69–71] proposed schemes to realize robust unconventional pumping with vdW- and DD-type RRI, respectively. These schemes may also be feasible to accomplish the same quantum information tasks that can be accomplished by the RAB regimes.

Conclusion. – In this paper, we have reviewed the RAB regimes with different RRI types and strength, and showed their applications, which may provide a reference for studying the RAB and RAB-based quantum technology. To achieve the RAB, the RAB condition should be satisfied accurately, which may be a challenge for the experiment since the interatomic distance would fluctuate due to the thermal noise. Thus, the future study may be focused on how to deal with the phonon modes. On the other hand, since the two- and multi-excitation Rydberg states would be populated in the RAB, the spontaneous emission of Rydberg states would no doubt decrease the

performance of the RAB-based schemes. To address this issue, one can choose Rydberg states with higher principal quanutm number that have long lifetime or enhance the coupled Rabi frequency suitably to minimize the evolution time. In addition, studying the RAB in the many-body system would also be another interesting topic [43,56,57,62].

$$* * *$$

REFERENCES

[1] GALLAGHER T. F., *Rydberg Atoms*, Vol. **3** (Cambridge University Press) 2005.

[2] SAFFMAN M., WALKER T. G. and MØLMER K., *Rev. Mod. Phys.*, **82** (2010) 2313.

[3] JAKSCH D., CIRAC J. I., ZOLLER P., ROLSTON S. L., CÔTÉ R. and LUKIN M. D., *Phys. Rev. Lett.*, **85** (2000) 2208.

[4] LUKIN M. D., FLEISCHHAUER M., COTE R., DUAN L. M., JAKSCH D., CIRAC J. I. and ZOLLER P., *Phys. Rev. Lett.*, **87** (2001) 037901.

[5] SAFFMAN M., *J. Phys. B: At. Mol. Opt. Phys.*, **49** (2016) 202001.

[6] COMPARAT D. and PILLET P., *J. Opt. Soc. Am. B*, **27** (2010) A208.

[7] BÉGUIN L., VERNIER A., CHICIREANU R., LAHAYE T. and BROWAEYS A., *Phys. Rev. Lett.*, **110** (2013) 263201.

[8] JAKSCH D., CIRAC J. I., ZOLLER P., ROLSTON S. L., CÔTÉ R. and LUKIN M. D., *Phys. Rev. Lett.*, **85** (2000) 2208.

[9] URBAN E., JOHNSON T. A., HENAGE T., ISENHOWER L., YAVUZ D., WALKER T. and SAFFMAN M., *Nat. Phys.*, **5** (2009) 110.

[10] GAËTAN A., MIROSHNYCHENKO Y., WILK T., CHOTIA A., VITEAU M., COMPARAT D., PILLET P., BROWAEYS A. and GRANGIER P., *Nat. Phys.*, **5** (2009) 115.

[11] ISENHOWER L., URBAN E., ZHANG X. L., GILL A. T., HENAGE T., JOHNSON T. A., WALKER T. G. and SAFFMAN M., *Phys. Rev. Lett.*, **104** (2010) 010503.

[12] ZHANG X. L., ISENHOWER L., GILL A. T., WALKER T. G. and SAFFMAN M., *Phys. Rev. A*, **82** (2010) 030306.

[13] WILK T., GAËTAN A., EVELLIN C., WOLTERS J., MIROSHNYCHENKO Y., GRANGIER P. and BROWAEYS A., *Phys. Rev. Lett.*, **104** (2010) 010502.

[14] MALLER K. M., LICHTMAN M. T., XIA T., SUN Y., PIOTROWICZ M. J., CARR A. W., ISENHOWER L. and SAFFMAN M., *Phys. Rev. A*, **92** (2015) 022336.

[15] ZENG Y., XU P., HE X., LIU Y., LIU M., WANG J., PAPOULAR D. J., SHLYAPNIKOV G. V. and ZHAN M., *Phys. Rev. Lett.*, **119** (2017) 160502.

[16] PICKEN C. J., LEGAIE R., MCDONNELL K. and PRITCHARD J. D., *Quantum Sci. Technol.*, **4** (2018) 015011.

[17] LEVINE H., KEESLING A., OMRAN A., BERNIEN H., SCHWARTZ S., ZIBROV A. S., ENDRES M., GREINER M.,

VULETI Ć V. and LUKIN M. D., *Phys. Rev. Lett.*, **121** (2018) 123603.

[18] LEVINE H., KEESLING A., SEMEGHINI G., OMRAN A., WANG T. T., EBADI S., BERNIEN H., GREINER M., VULETIĆ V., PICHLER H. and LUKIN M. D., *Phys. Rev. Lett.*, **123** (2019) 170503.

[19] GRAHAM T. M., KWON M., GRINKEMEYER B., MARRA Z., JIANG X., LICHTMAN M. T., SUN Y., EBERT M. and SAFFMAN M., *Phys. Rev. Lett.*, **123** (2019) 230501.

[20] MADJAROV I. S., COVEY J. P., SHAW A. L., CHOI J., KALE A., COOPER A., PICHLER H., SCHKOLNIK V., WILLIAMS J. R. and ENDRES M., *Nat. Phys.*, **16** (2020) 857.

[21] ATES C., POHL T., PATTARD T. and ROST J. M., *Phys. Rev. Lett.*, **98** (2007) 023002.

[22] AMTHOR T., GIESE C., HOFMANN C. S. and WEIDEMÜLLER M., *Phys. Rev. Lett.*, **104** (2010) 013001.

[23] POHL T. and BERMAN P. R., *Phys. Rev. Lett.*, **102** (2009) 013004.

[24] QIAN J., QIAN Y., KE M., FENG X.-L., OH C. H. and WANG Y., *Phys. Rev. A*, **80** (2009) 053413.

[25] ZUO Z. and NAKAGAWA K., *Phys. Rev. A*, **82** (2010) 062328.

[26] LEE T. E., HÄFFNER H. and CROSS M. C., *Phys. Rev. Lett.*, **108** (2012) 023602.

[27] LI W., ATES C. and LESANOVSKY I., *Phys. Rev. Lett.*, **110** (2013) 213005.

[28] CARR A. W. and SAFFMAN M., *Phys. Rev. Lett.*, **111** (2013) 033607.

[29] SHAO X.-Q., YOU J.-B., ZHENG T.-Y., OH C. H. and ZHANG S., *Phys. Rev. A*, **89** (2014) 052313.

[30] SU S.-L., GUO Q., WANG H.-F. and ZHANG S., *Phys. Rev. A*, **92** (2015) 022328.

[31] ZHAO Y. J., LIU B., JI Y. Q., TANG S. Q. and SHAO X. Q., *Sci. Rep.*, **7** (2017) 16489.

[32] SHAO X. Q., WU J. H., YI X. X. and LONG G.-L., *Phys. Rev. A*, **96** (2017) 062315.

[33] CHEN Y.-H., SHI Z.-C., SONG J., XIA Y. and ZHENG S.-B., *Phys. Rev. A*, **97** (2018) 032328.

[34] CHEN X., XIE H., LIN G.-W., SHANG X., YE M.-Y. and LIN X.-M., *Phys. Rev. A*, **96** (2017) 042308.

[35] LI D.-X., SHAO X.-Q., WU J.-H. and YI X. X., *Opt. Lett.*, **43** (2018) 1639.

[36] LI D.-X., SHAO X.-Q., WU J.-H., YI X. X. and ZHENG T.-Y., *Opt. Express*, **26** (2018) 2292.

[37] LI D. X. and SHAO X. Q., *Phys. Rev. A*, **99** (2019) 032348.

[38] YANG C., LI D. and SHAO X., *Sci. China Phys. Mech.*, **62** (2019) 110312.

[39] LI R., YU D., SU S.-L. and QIAN J., *Phys. Rev. A*, **101** (2020) 042328.

[40] BASAK S., CHOUGALE Y. and NATH R., *Phys. Rev. Lett.*, **120** (2018) 123204.

[41] SU S.-L., LIANG E., ZHANG S., WEN J.-J., SUN L.-L., JIN Z. and ZHU A.-D., *Phys. Rev. A*, **93** (2016) 012306.

[42] SU S.-L., TIAN Y., SHEN H. Z., ZANG H., LIANG E. and ZHANG S., *Phys. Rev. A*, **96** (2017) 042335.

[43] SU S. L., SHEN H. Z., LIANG E. and ZHANG S., *Phys. Rev. A*, **98** (2018) 032306.

[44] ZHU X.-Y., LIANG E. and SU S.-L., *J. Opt. Soc. Am. B*, **36** (2019) 1937.

[45] WU J.-L., SONG J. and SU S.-L., *Phys. Lett. A*, **384** (2020) 126039.

[46] WU J.-L., SU S.-L., WANG Y., SONG J., XIA Y. and JIANG Y.-Y., *Opt. Lett.*, **45** (2020) 1200.

[47] SU S.-L., GUO F.-Q., TIAN L., ZHU X.-Y., YAN L.-L., LIANG E.-J. and FENG M., *Phys. Rev. A*, **101** (2020) 012347.

[48] XING T. H., WU X. and XU G. F., *Phys. Rev. A*, **101** (2020) 012306.

[49] SU S.-L., GAO Y., LIANG E. and ZHANG S., *Phys. Rev. A*, **95** (2017) 022319.

[50] BETEROV I. I., SAFFMAN M., YAKSHINA E. A., TRETYAKOV D. B., ENTIN V. M., BERGAMINI S., KUZNETSOVA E. A. and RYABTSEV I. I., *Phys. Rev. A*, **94** (2016) 062307.

[51] TRETYAKOV D. B., BETEROV I. I., YAKSHINA E. A., ENTIN V. M., RYABTSEV I. I., CHEINET P. and PILLET P., *Phys. Rev. Lett.*, **119** (2017) 173402.

[52] BETEROV I. I., ASHKARIN I. N., YAKSHINA E. A., TRETYAKOV D. B., ENTIN V. M., RYABTSEV I. I., CHEINET P., PILLET P. and SAFFMAN M., *Phys. Rev. A*, **98** (2018) 042704.

[53] BAI S., TIAN X., HAN X., JIAO Y., WU J., ZHAO J. and JIA S., *New J. Phys.*, **22** (2020) 013004.

[54] GAMBETTA F. M., ZHANG C., HENNRICH M., LESANOVSKY I. and LI W., *Long-range multi-body interactions and three-body anti-blockade in a trapped Rydberg ion chain*, arXiv:2005.05726 (2020).

[55] TAYLOR J., SINCLAIR J., BONSMA-FISHER K., ENGLAND D., SPANNER M. and HESHAMI K., *Generation of doubly excited Rydberg states based on Rydberg antiblockade in a cold atomic ensemble*, arXiv:1912.05675 (2019).

[56] GAMBETTA F. M., LI W., SCHMIDT-KALER F. and LESANOVSKY I., *Phys. Rev. Lett.*, **124** (2020) 043402.

[57] MAZZA P. P., SCHMIDT R. and LESANOVSKY I., *Phys. Rev. Lett.*, **125** (2020) 033602.

[58] SHI X.-F., *Phys. Rev. Appl.*, **7** (2017) 064017.

[59] SHI X.-F., *Phys. Rev. Appl.*, **11** (2019) 044035.

[60] KASTORYANO M. J., REITER F. and SØRENSEN A. S., *Phys. Rev. Lett.*, **106** (2011) 090502.

[61] RAO D. D. B. and MØLMER K., *Phys. Rev. Lett.*, **111** (2013) 033606.

[62] GÄRTTNER M., HEEG K. P., GASENZER T. and EVERS J., *Phys. Rev. A*, **88** (2013) 043410.

[63] YOUNG J. T., BOULIER T., MAGNAN E., GOLDSCHMIDT E. A., WILSON R. M., ROLSTON S. L., PORTO J. V. and GORSHKOV A. V., *Phys. Rev. A*, **97** (2018) 023424.

[64] OSTMANN M., MARCUZZI M., MINÁŘ J. and LESANOVSKY I., *Quantum Sci. Technol.*, **4** (2019) 02LT01.

[65] SU S.-L., *Rydberg antiblockade with resonant dipole-dipole interactions*, arXiv:2006.06529 (2020).

[66] GUÉRY-ODELIN D., RUSCHHAUPT A., KIELY A., TORRONTEGUI E., MARTÍNEZ-GARAOT S. and MUGA J. G., *Rev. Mod. Phys.*, **91** (2019) 045001.

[67] SHEN C.-P., WU J.-L., SU S.-L. and LIANG E., *Opt. Lett.*, **44** (2019) 2036.

[68] KANG Y.-H., CHEN Y.-H., SHI Z.-C., HUANG B.-H., SONG J. and XIA Y., *Phys. Rev. A*, **97** (2018) 042336.

[69] LI D. X. and SHAO X. Q., *Phys. Rev. A*, **98** (2018) 062338.

[70] SHAO X.-Q., *Selective Rydberg pumping via strong dipole blockade*, arXiv:2006.10989 (2020).

[71] ZHENG R.-H., KANG Y.-H., SU S.-L., SONG J. and XIA Y., *Phys. Rev. A*, **102** (2020) 012609.